A Switched-capacitor Step-up Inverter for Bidirectional Wireless Charging Applications in Electric Microcar

Fong Y. C [1]   Cheng K. W. E [2]

Abstract–Wireless power transfer (WPT) offers a more convenient and safer option for electric vehicle (EV) charging. However, the mismatch of the DC link voltages between the charging stations and small scale EVs may increase the difficulty of design and control of the charging facilities. Along with the growing penetration of renewable energy, vehicle-to-buildings (V2B) and vehicle-to-grid (V2G) interfaces, requiring bidirectional power flow would be the essential features of future EV wireless charging systems. In order to tackle this issue, this paper suggests a high-frequency step-up inverter based on series-parallel conversion of switched-capacitor with the associated staircase modulation and power flow control for WPT applications. Corresponding to the system parameters of a typical electric microcars, the operating principle and the power flow control of the proposed inverter are verified by simulation. The battery power as well as the primary and secondary AC waveforms of the simulation model are presented.

Keywords–Electric vehicle (EV) charging, inductive power transfer (IPT), DC-AC power converters, switched-capacitor circuits.

I. Introduction

Wireless power transfer (WPT) is one of the emerging technologies for powering consumer electronics, portable devices and even electric vehicles (EVs). This technology greatly improves the convenience and safety, as well as enables a wide range of commercial, industrial and medical applications like electrified transportations, industrial robots, sensor networks and biomedical implants [1-9]. Inductive power transfer (IPT) is a promising and well developed technology for short to mid-range wireless applications including wireless charging for EVs. Last year, the Society of Automotive Engineers (SAE) has released the wireless charging standard, TIR J2954 [10], for light duty plug-in hybrid EVs or EVs that utilizes a common frequency band of around 80kHz to 90kHz for inductive power transfer at power levels of a few kilowatts to dozen-kilowatts. Fig. 1 illustrates a typical wireless EV charging system based on IPT [11]. The transmitter side, supplied by AC voltage source from the utility, usually consists of a power factor correction (PFC) rectifier following a high-frequency inverter to convert the output frequency and voltage level. Since the coupling factor would be very low for WPT, compensation networks would be required for both primary and secondary coils to compensate the leakage inductance which improve the power factor as well as the energy efficiency. In the receiving side, diode bridge rectifier is most commonly used to convert the high-frequency AC waveform to DC

[1, 2] **Power Electronics Research Centre, Department of Electrical Engineering**
The Hong Kong Polytechnic University, Hong Kong
[1]**E-mail:** yc-chi.fong@connect.polyu.hk

waveform and filter the voltage and current ripples with capacitor or inductor-capacitor filter.

However, the use of diode rectifier in the receiving end restricts the direction of power flow. In the conventional design, only charging operation, i.e. charging from the utility supply to the vehicle energy storage system (ESS), is permitted. This would deny the benefits provided by these grid-enable vehicles (GEVs) and sway the future implementation and development on the EV related features in smart-grid and micro-grid such as the vehicle-to-buildings (V2B) and vehicle-to-grid (V2G) applications [12]. The literature indicates that the GEVs would play a very important role in the future utility since the intelligent energy interface between the utility and the vehicles' ESSs could smooth the power pattern, support the increasing penetration of renewable energy, and even provide ancillary services to regulate the grid voltage and frequency [12-15].

The feature of bidirectional power flow could be enabled by simply substitute the diode rectifier in the receiver with inverter (Fig. 2). There are some wireless charging system designs [16-18] employing H-bridge as the pick-up converter in the receiving end for providing bidirectional power flow. However, these designs require a relative high battery voltage since the DC link voltage supplied by the PFC rectifier at the primary side could be up to several hundred-volts and the DC link voltage at the pick-up side should be in the same order of magnitude to facilitate bidirectional power flow. For small vehicles such as microcars having comparative low battery voltage, the large mismatch between the battery voltage and the DC link voltage at the charging station would increase the design and control difficulty of the charging components. For this reason, a bidirectional DC-DC converter or a step-up inverter would be required in this situation.
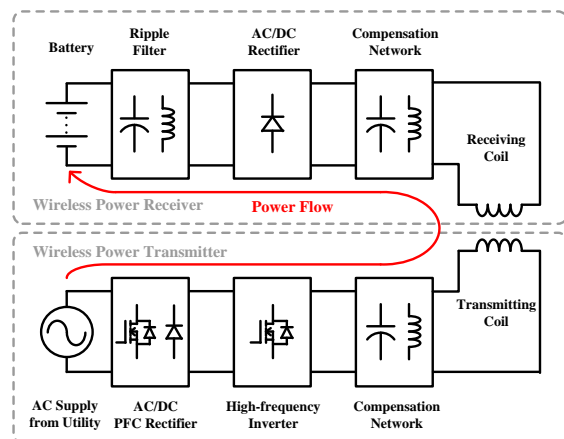

Fig. 1: A typical unidirectional wireless EV charging system based on IPT
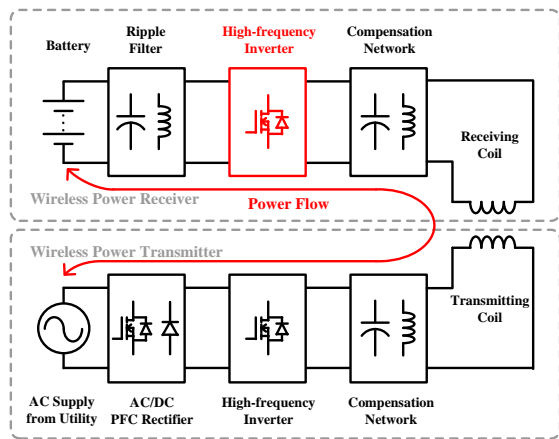
Fig. 2: A bidirectional wireless EV charging system with a high-frequency inverter in the receiver

Table I: The switching table for a 7-level SCMLI*

V_o	$C_{1a}, C_{2a}, C_{1b}, C_{2b}$	$S_{31a}, S_{32a}, S_{31b}, S_{32b}$
0	P, P, P, P	1, 0, 1, 0
V_{dc}	S, P, P, P	1, 0, 1, 0
$2V_{dc}$	S, S, P, P	1, 0, 1, 0
$3V_{dc}$	S, S, P, P	0, 1, 1, 0
$2V_{dc}$	P, S, P, P	0, 1, 1, 0
V_{dc}	P, P, P, P	0, 1, 1, 0
0	P, P, P, P	1, 0, 1, 0
$-V_{dc}$	P, P, S, P	1, 0, 1, 0
$-2V_{dc}$	P, P, S, S	1, 0, 1, 0
$-3V_{dc}$	P, P, S, S	1, 0, 0, 1
$-2V_{dc}$	P, P, P, S	1, 0, 0, 1
$-V_{dc}$	P, P, P, P	1, 0, 0, 1
0	P, P, P, P	1, 0, 1, 0

*S: Series; P: Parallel

The switched-capacitor (SC) multilevel inverter (MLI) has received more attention in recently years. This type of inverters offer voltage step-up capability and self-balancing of capacitor voltage by the technique of series-parallel conversion [19-22]. In addition, the topology presented in [19] has demonstrated the capability of SCMLI for driving inductive load; the topology suggested in [22] reduces the ratings of components by eliminating the need of H-bridge back-end. The mathematical analyses on the voltage ripples of the switched-capacitors and the energy efficiency in previous research have indicated that this type of inverters are more favorable for high-frequency applications. As the capacitor sizes are essentially inversely proportional to the operating frequency, the switched-capacitor inverters would be the ideal candidates for WPT applications working at around 80kHz.

In this paper, a SCMLI offering bidirectional power flow and voltage step-up capability, based on the principle of series-parallel conversion, is proposed for WPT applications. The operation principle of the topology as well as the modulation and power flow control will be described. The simulation of a model, based on the applications for light-duty microcars with comparatively low battery voltage, has been conducted and the corresponding results will be presented.
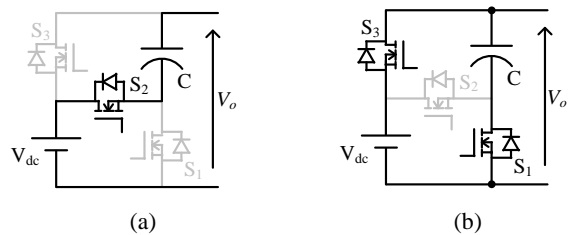

Fig. 3: Series-parallel conversion of an SC cell; (a) series operation; (b) parallel operation
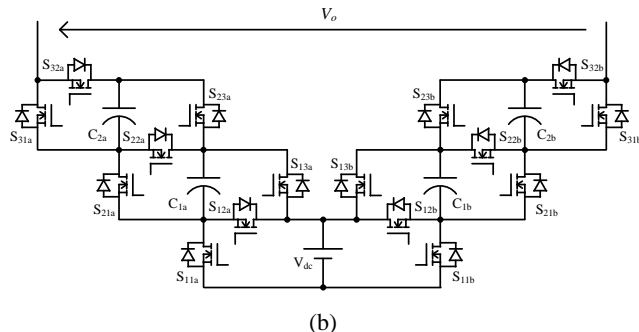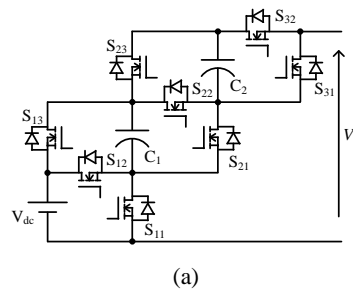

(a)

(b)

Fig. 4: The proposed switched-capacitor multilevel inverter; (a) one phase of SC converter with two SC cells; (b) a 7-level SCMLI formed by two SC converters

II. OPERATION PRINCIPLE OF THE INVERTER

1. General Description

The proposed topology is derived from the series-parallel conversion of switched-capacitor. The basic operation of an SC cell is depicted in Fig. 3. When S_1 and S_3 are conducted, the capacitor would be charged to the same voltage level as the voltage source; when only S_2 is conducted, the voltage level across the SC cell is doubled by connecting the capacitor and the voltage source in-series. One phase of SC converter, consists of two SC cells, and the proposed 7-level SCMLI, consists of two phases of SC converters, are illustrated in Fig. 4(a) and 4(b), respectively. By sequentially series and parallel switching of the SC cells, multilevel voltage waveforms could be produced at the output terminal of an SC converter phase; by applying time (phase angle) shift between two phases, bipolar multilevel voltage waveforms are produced across the terminals of different phases. As the switches for both series and parallel operations allow current flow of both directions at on-state, the capacitors could be charged by both DC bus and AC bus. Therefore, the proposed SCMLI topology is capable of handling power flow in both directions.

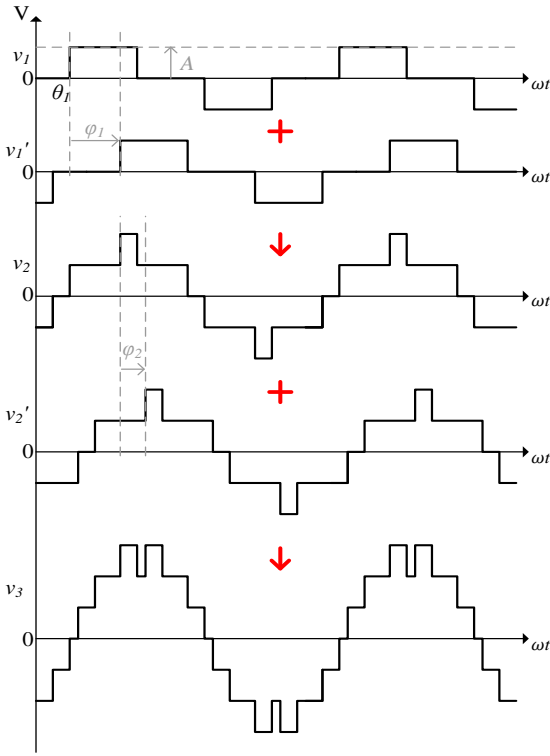In the proposed topology, bipolar output voltage waveforms are produced by the phase angle difference

Fig. 5: Synthesis of 7-level staircase voltage waveform based on phase-shift and superposition

between the SC converters. In each of the SC converters, the voltage stresses of the active switches are limited by the operating voltage of the SC cells, which is about the same magnitude as the DC bus. By eliminating the need of the high voltage H-bridge, the maximum voltage ratings of the semiconductor switches are greatly reduced comparing to the designs suggested in [19-21]. A table of switching states for different output voltage level for a 7-level inverter is listed in table I. The operation of the proposed topology is time interleaved by adopting the multiphase structure. A much longer parallel duration for capacitor charging is provided, therefore, a significantly higher maximum operating frequency would be allowed, compared to the existing SCMLIs suggested in [19-22].

2. Staircase Modulation with Phase-shift Harmonic Elimination Technique

Considering that the switching losses of the inverter are roughly proportional to the switching frequency, the switching losses would be too high if high frequency modulation method like the level-shifted or phase-shifted PWM is employed. For the high-frequency applications such as WPT, staircase modulation methods working at the fundamental output frequency are preferred. As shown in Fig. 2, the IPT system consists of compensation networks in both primary and secondary sides. The compensation networks could form band-pass filters with the self or leakage inductance of the transmitting or receiving coils. When operating near the resonant frequency, the roll-off of the band-pass filters would be fast enough to filter most of the high-frequency harmonic contents.

Selective harmonic elimination (SHE) [23] is one of the most common fundamental frequency modulation techniques for multilevel inverter. The SHE technique computes the firing angles for a specific modulation index

and eliminating the selected harmonic contents, usually the lowest order harmonics, by solving a system of nonlinear equations. SHE is effective generating the required staircase voltage waveforms which precisely preserves the amplitude of fundamental component and rejects the low order harmonics, yet the conventional SHE method demands a lot of computation which is time consuming and difficult to be implemented in real-time [24-25]. Instead of solving a system of nonlinear equations, a simpler phase-shift technique is employed in this study to compute the firing angles.

Fig. 5 explains the synthesis of 7-level staircase voltage waveform based on the phase-shift harmonic elimination technique. v_1 represents the one-step voltage waveform and v_1' is the phase-shifted waveform of v_1. v_2 is the two-step voltage waveform synthesized by superposing v_1 and v_1'. Similarly, v_2' is the phase-shifted waveform of v_2; v_3 is synthesized from v_2 and v_2'. If the firing angle of v_1 is θ_1, based on Fourier analysis, the amplitudes of the fundamental voltage as well as the harmonics would be

$$A_{1,n} = \frac{4A}{n\pi}\cos(n\theta_1) \tag{1}$$

where $n = 1, 3, 5, ...$, is the harmonic order ($n = 1$ represents the fundamental component). By phase-shifting v_1 by φ_1 and superposing to itself, the Fourier coefficients of the resultant waveform v_2, would be

$$A_{2,n} = \frac{8A}{n\pi}\cos(n\theta_1)\sin\left(\frac{\pi + n\varphi_1}{2}\right) \tag{2}$$

Similarly, by phase-shifting v_2 by φ_1 and superposing them again, the decomposed amplitudes of v_3 would be

$$A_{3,n} = \frac{16A}{n\pi}\cos(n\theta_1)\sin\left(\frac{\pi + n\varphi_1}{2}\right)\sin\left(\frac{\pi + n\varphi_2}{2}\right) \tag{3}$$

By means of putting the specific harmonics to zero, i.e.

$$\begin{cases} \sin\left(\frac{\pi + n_1\varphi_1}{2}\right) = 0 \\ \sin\left(\frac{\pi + n_2\varphi_2}{2}\right) = 0 \end{cases} \tag{4}$$

the corresponding harmonic contents could be eliminated easily. The fundamental amplitude of the resultant waveform, v_3, could be expressed as (5).

$$A_{3,1} = \frac{16A}{\pi}\cos(\theta_1)\sin\left(\frac{\pi + \varphi_1}{2}\right)\sin\left(\frac{\pi + \varphi_2}{2}\right) \tag{5}$$

By definition, the modulation index, m, for the 7-level MLI is
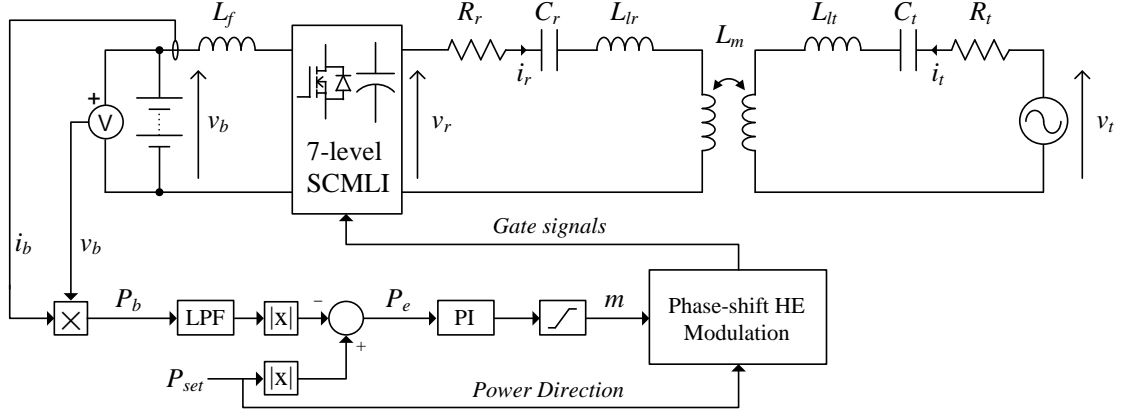
$$m = \frac{\pi A_{3,1}}{12V_{dc}} \tag{6}$$

Fig. 7: Schematic for the configuration of the simulation model

By putting (5) into (6), the modulation index of the 7-level inverter could be a function of θ_1, φ_1 and φ_2, i.e.

$$m = \frac{4}{3}\cos(\theta_1)\sin\left(\frac{\pi+\varphi_1}{2}\right)\sin\left(\frac{\pi+\varphi_2}{2}\right) \tag{7}$$

As φ_1 and φ_2 would be constant values for eliminating predefined harmonics, the sine terms could be calculated offline. Thus, the modulation index of the inverter could be controlled by the firing angle, θ_1, easily.

Since v_3 is synthesized by superposing two two-step voltage waveforms, the maximum number of steps would be four. In order to limit the maximum number of steps of v_3 to three, the following criteria should be fulfilled.

$$\theta_1 + \varphi_1 + \varphi_2 > \pi - \theta_1$$
$$\theta_1 > \frac{\pi - \varphi_1 - \varphi_2}{2} \tag{8}$$

Therefore, the maximum modulation index for the 7-level MLI, which eliminates two sets of harmonics by the phase-shift harmonic elimination technique, would be limited such that

$$m < \frac{4}{3}\cos\left(\frac{\pi-\varphi_1-\varphi_2}{2}\right)\sin\left(\frac{\pi+\varphi_1}{2}\right)\sin\left(\frac{\pi+\varphi_2}{2}\right) \tag{9}$$

For example, if the 3rd, 9th,... and 5th, 15th,... harmonics are eliminated, the maximum attainable modulation index, m_{max}, would be

$$m_{\max} = \frac{4}{3}\cos\left(\frac{7\pi}{30}\right)\sin\left(\frac{2\pi}{3}\right)\sin\left(\frac{3\pi}{5}\right)$$
$$\approx 0.8161 \tag{10}$$

3. Power Flow Control

LC-series structure is one of the most basic compensation configurations for IPT systems. The equivalent circuit for a series-series compensation network is depicted in Fig. 6. v_p and v_s are the output voltage of the inverters at primary side and secondary side, respective. C_p, R_p, C_s, and R_s are the compensation capacitances and the equivalent series resistance for the primary and secondary coils. L_{lp}, L_{ls} and

L_m are the primary leakage inductance, secondary leakage inductance and mutual inductance of the transmission coils, i.e. $L_p = L_{lp} + L_m$ and $L_s = L_{ls} + L_m$.

The real and reactive power from the primary side could be evaluated by the following

$$\begin{cases} P = \mathrm{Re}(v_p i_p{}^*) \\ Q = \mathrm{Im}(v_p i_p{}^*) \end{cases} \tag{11}$$

If the self-inductance of the primary and secondary coils are compensated at the same resonant frequency and both the primary and secondary inverters operate at the resonant frequency, i.e.

$$\omega = \frac{1}{\sqrt{L_p C_p}} = \frac{1}{\sqrt{L_s C_s}} \tag{12}$$

The input power at the primary side could be derived as the following [26]

$$\begin{cases} P = -\frac{V_p V_s}{2L_m \omega}\sin\delta \\ Q = -\frac{V_p V_s}{2L_m \omega}\cos\delta \end{cases} \tag{13}$$

where, V_p and V_s are the fundamental amplitudes of the primary and secondary voltages, and δ is the phase angle difference. Referring to (13) the magnitudes of the real and reactive power could be controlled by the modulation index, while the power factor as well as the direction of power flow could be controlled by the phase-shift. Also, the maximum power factor and efficiency would be attained when the phase-shift is $\pm\pi/2$.
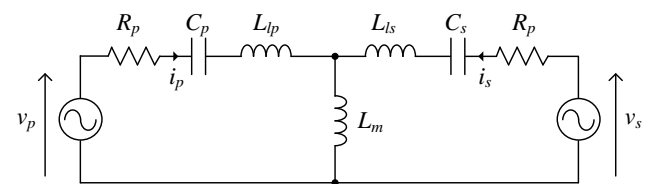

Fig. 6: The equivalent circuit for IPT with series-series LC compensation network

Table II: Parameters of the simulation model

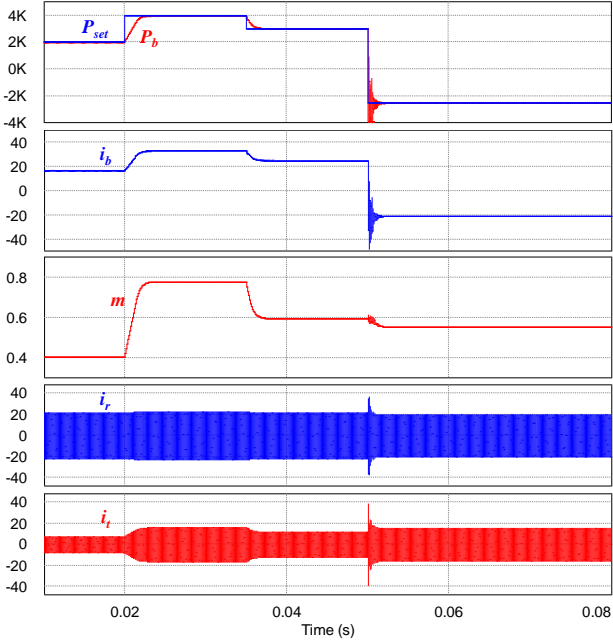| Parameter	Value
Battery voltage (V_b)	120V
Secondary AC source	$400V_{peak}$
Filter inductor (L_f)	10μH, 10mΩ
Switched-capacitors	10μF, 50mΩ
MOSFET $R_{ds(on)}$	50mΩ
R_1, R_2	1.5Ω
C_1, C_2	20nF
L_{l1}, L_{l2}	144μH
L_m	36μH
Operating frequency	84kHz

Fig. 8: Simulated waveforms of the models; the battery power, P_b, and power set-point, P_{set}; battery current, i_b; modulation index, m; current of the primary and secondary coils, i_r and i_t

Fig. 9: The AC waveforms and the corresponding switched-capacitor voltage at around t = 0.03s; the output voltage, v_r, and current, i_r, of the 7-level SCMLI; the secondary coil current, i_t, and AC source voltage, v_t; the voltage of the switched-capacitor C_{1b} and C_{2b}

Fig. 10: Fast Fourier transform (FFT) of the output voltage, v_r, and current, i_r, of the 7-level SCMLI

III. VERIFICATIONS

In order to verify the operation of the proposed topology, a simulation model of an IPT system, employing the 7-level SCMLI at one side, was implemented. The magnitude of the real power was controlled by PI compensation; the battery power was calculated form the instantaneous battery voltage and current, and the calculated power was compared with the power set-point; the error was inputted to the PI controller which generated the required modulation index. The direction of power flow was determined by the phase angle, which could be either π/2 or –π/2. Fig. 7 illustrates the simulation set-up; the associated parameters are shown in table II.

In the simulation model, the battery voltage, v_b, was 120V. The voltage was stepped-up and inverted by the 7-level SCMLI, the capacitance of each of the switched-capacitor was 10μF. The power was transmitted through the inductive coils with self-inductance of 180μH which were compensated by series capacitors. In the secondary side, an AC voltage source of 400V peak voltage was used to simulate the inverter output at the charging pad. The operating frequency of the simulated IPT system was 84kHz such that the compensation capacitance was
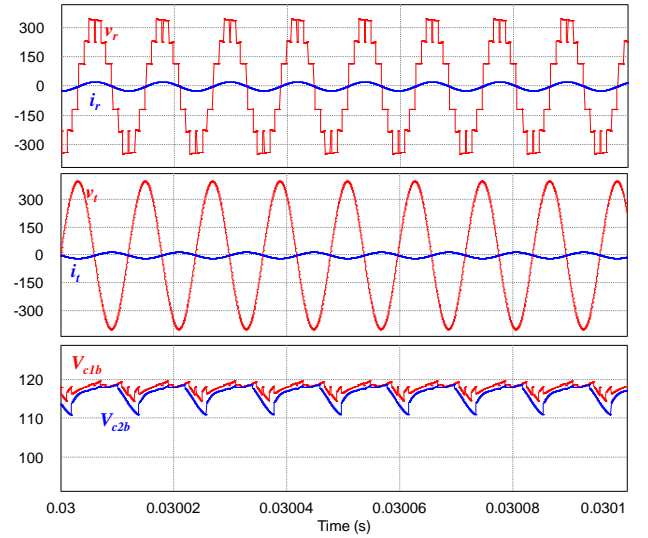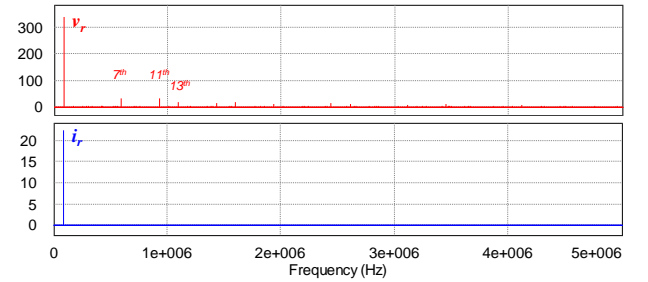
resonated with the self-inductance of the coils. The simulated waveforms are illustrated in Fig. 8. At the beginning, the power set-point for the battery was 2000W, then, it was doubled at *t = 0.02s*; and then declined to 3000W at *t = 0.035s*. At *t = 0.05s*, the battery was altered to charging mode by setting the power to −2000W. As shown in the results, the simulated battery power would able to track the set-point value and control the power flow with the aforementioned technique. In addition, a few cycles of power oscillating was observed at the instant of change in direction. It was due to the fact that the phase change was applied during non-zero current. This issue could be improved if the controller could apply the π-shift at zero-current by zero-crossing detection and soft-altering. Furthermore, the inverter output waveforms at around *t = 0.03s*, generated by the phase-shift harmonic elimination technique are illustrated in Fig. 9. From the corresponding fast Fourier transform (FFT) shown in Fig. 10, it could be observed that the 3rd, 9th,… and 5th, 15th,…, voltage harmonics were removed; and most of the remaining harmonics were effectively filtered by the resonant circuit. At P_b = 4000W, the voltage ripples of the capacitors was only about 8% of the charging voltage, this suggested that the proposed SCMLI with the above-mentioned parameters would be capable of WPT applications at a few kilowatts.

IV. CONCLUSION

A high-frequency inverter for WPT applications based on the series-parallel conversion technique is presented. The voltage step-up feature improves the capability of bidirectional power flow without the need of DC-DC converter stage in small vehicles having relative low battery voltage like microcars. The presented modulation and control techniques are easily to implement and effective for high-frequency applications like IPT. With the built-in resonant tanks, the inverter could achieve satisfactory power quality with simple harmonic elimination technique. The topology as well as the operation principles of the proposed inverter was verified by simulation. Comparing to the conductive applications, the SCMLI is capable of higher power level at small capacitor sizes due to the substantial increase in frequency.

ACKNOWLEDGMENT

REFERENCES

[1] A. Kawamura, K. Ishioka and J. Hirai, "Wireless transmission of power and information through one high-frequency resonant AC link inverter for robot manipulator applications," in *IEEE Trans. on Ind. Appl.*, vol. 32, no. 3, pp. 503-508, May/Jun 1996.

[2] K. O'Brien, G. Scheible and H. Gueldner, "Analysis of wireless power supplies for industrial automation systems," *Ind. Electron. Society, 2003. IECON '03. The 29th Annual Conf. of the IEEE*, 2003, pp. 367-372 vol.1.

[3] S. Y. R. Hui and W. W. C. Ho, "A new generation of universal contactless Battery Charging platform for portable Consumer Electronic equipment," in *IEEE Trans. on Power Electron.*, vol. 20, no. 3, pp. 620-627, May 2005.

[4] C. H. Hu, C. M. Chen, Y. S. Shiao, T. J. Chan and T. R. Chen, "Development of a universal contactless charger for handheld devices," *2008 IEEE Int. Symp. on Ind. Electron.*, Cambridge, 2008, pp. 99-104.

[5] G. A. Covic and J. T. Boys, "Modern Trends in Inductive Power Transfer for Transportation Applications," in *IEEE Journal of Emerging and Selected Topics in Power Electron.*, vol. 1, no. 1, pp. 28-41, March 2013.

[6] O. C. Onar, J. M. Miller, S. L. Campbell, C. Coomer, C. P. White and L. E. Seiber, "A novel wireless power transfer for in-motion EV/PHEV charging," *2013 Twenty-Eighth Annual IEEE Applied Power Electron. Conf. and Exposition (APEC)*, Long Beach, CA, USA, 2013, pp. 3073-3080.

[7] Q. Xu, H. Wang, Z. Gao, Z. H. Mao, J. He and M. Sun, "A Novel Mat-Based System for Position-Varying Wireless Power Transfer to Biomedical Implants," in *IEEE Trans. on Magnetics*, vol. 49, no. 8, pp. 4774-4779, Aug. 2013.

[8] M. Erol-Kantarci and H. T. Mouftah, "Suresense: sustainable wireless rechargeable sensor networks for the smart grid," in *IEEE Wireless Communications*, vol. 19, no. 3, pp. 30-36, June 2012.

[9] G. Covic and J. Boys, "Inductive power transfer," *Proc. IEEE*, vol. 101, no. 6, pp. 1276–1289, Jun. 2013.

[10] (2017). [Online]. Available: standards.sae.org/wip/j2954/

[11] B. Esteban, M. Sid-Ahmed and N. C. Kar, "A Comparative Study of Power Supply Architectures in Wireless EV Charging Systems," in *IEEE Trans. on Power Electron.*, vol. 30, no. 11, pp. 6408-6422, Nov. 2015.

[12] A. G. Boulanger, A. C. Chu, S. Maxx and D. L. Waltz, "Vehicle Electrification: Status and Issues," in *Proc. of the IEEE*, vol. 99, no. 6, pp. 1116-1138, June 2011.

[13] W. Su, H. Eichi, W. Zeng and M. Y. Chow, "A Survey on the Electrification of Transportation in a Smart Grid Environment," in *IEEE Trans. on Ind. Informatics*, vol. 8, no. 1, pp. 1-10, Feb. 2012.

[14] H. N. T. Nguyen, C. Zhang and M. A. Mahmud, "Optimal Coordination of G2V and V2G to Support Power Grids With High Penetration of Renewable Energy," in *IEEE Trans. on Transportation Electrification*, vol. 1, no. 2, pp. 188-195, Aug. 2015.

[15] Y. He, B. Venkatesh and L. Guan, "Optimal Scheduling for Charging and Discharging of Electric Vehicles," in *IEEE Trans. on Smart Grid*, vol. 3, no. 3, pp. 1095-1105, Sept. 2012.

[16] J. Y. Lee and B. M. Han, "A Bidirectional Wireless Power Transfer EV Charger Using Self-Resonant PWM," in *IEEE Trans. on Power Electron.*, vol. 30, no. 4, pp. 1784-1787, April 2015.

[17] L. Zhao, D. J. Thrimawithana and U. K. Madawala, "Hybrid Bidirectional Wireless EV Charging System Tolerant to Pad Misalignment," in *IEEE Trans. on Ind. Electron.*, vol. 64, no. 9, pp. 7079-7086, Sept. 2017.

[18] A. A. S. Mohamed, A. Berzoy, F. G. N. de Almeida and O. Mohammed, "Modeling and Assessment Analysis of Various Compensation Topologies in Bidirectional IWPT System for EV Applications," in *IEEE Trans. on Ind. Appl.*, vol. 53, no. 5, pp. 4973-4984, Sept.-Oct. 2017.

[19] Y. Hinago and H. Koizumi, "A Switched-Capacitor Inverter Using Series/Parallel Conversion With Inductive Load," in *IEEE Trans. on Ind. Electron.*, vol. 59, no. 2, pp. 878-887, Feb. 2012.

[20] Y. Ye, K. W. E. Cheng, J. Liu and K. Ding, "A Step-Up Switched-Capacitor Multilevel Inverter With Self-Voltage Balancing," in *IEEE Trans. on Ind. Electron.*, vol. 61, no. 12, pp. 6672-6680, Dec. 2014.

[21] E. Zamiri, N. Vosoughi, S. H. Hosseini, R. Barzegarkhoo and M. Sabahi, "A New Cascaded Switched-Capacitor Multilevel Inverter Based on Improved Series–Parallel Conversion With Less Number of Components," in *IEEE Trans. on Ind. Electron.*, vol. 63, no. 6, pp. 3582-3594, June 2016.

[22] Y. C. Fong, S. Raghu Raman, M. Moonson Chen and K.W.E. Cheng, "A Novel Switched-capacitor Multilevel Inverter Offering Modularity in Design," *2018 IEEE Applied Power Electron. Conf. and Exposition (APEC)*, San Antonio, TX, 2018.

[23] J. R. Wells, B. M. Nee, P. L. Chapman and P. T. Krein, "Selective harmonic control: a general problem formulation and selected solutions," in *IEEE Trans. on Power Electron.*, vol. 20, no. 6, pp. 1337-1345, Nov. 2005.

[24] D. Ahmadi, K. Zou, C. Li, Y. Huang and J. Wang, "A Universal Selective Harmonic Elimination Method for High-Power Inverters," in *IEEE Trans. on Power Electron.*, vol. 26, no. 10, pp. 2743-2752, Oct. 2011.

[25] M. Ahmed, A. Sheir and M. Orabi, "Real-Time Solution and Implementation of Selective Harmonic Elimination of Seven-Level Multilevel Inverter," in *IEEE Journal of Emerging and Selected Topics in Power Electron.*, vol. 5, no. 4, pp. 1700-1709, Dec. 2017.

[26] A. A. S. Mohamed, A. Berzoy, F. G. N. de Almeida and O. Mohammed, "Modeling and Assessment Analysis of Various Compensation Topologies in Bidirectional IWPT System for EV Applications," in *IEEE Trans. on Ind. Appl.*, vol. 53, no. 5, pp. 4973-4984, Sept.-Oct. 2017.